

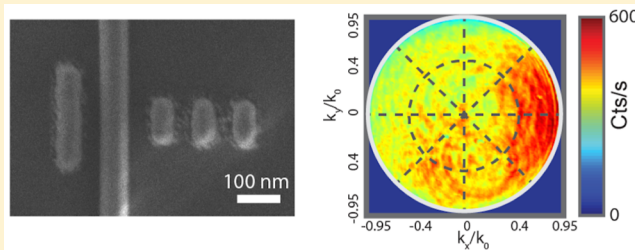
Hybrid Semiconductor Nanowire–Metallic Yagi-Uda Antennas

Mohammad Ramezani,^{†,‡} Alberto Casadei,[†] Grzegorz Grzela,[‡] Federico Matteini,[†] Gözde Tütüncüoğlu,[†] Daniel Ruffer,[†] Anna Fontcuberta i Morral,^{*,†} and Jaime Gómez Rivas^{*,‡,§}[†]Laboratoire des Matériaux Semiconducteurs, École Polytechnique Fédérale de Lausanne, 1015 Lausanne, Switzerland[‡]Center for Nanophotonics, FOM Institute AMOLF, c/o Philips Research Laboratories, High Tech Campus 4, 5656 AE Eindhoven, The Netherlands[§]COBRA Research Institute, Eindhoven University of Technology, P.O. Box 513, 5600 MB Eindhoven, The Netherlands

Supporting Information

ABSTRACT: We demonstrate the directional emission of individual GaAs nanowires by coupling this emission to Yagi-Uda optical antennas. In particular, we have replaced the resonant metallic feed element of the nanoantenna by an individual nanowire and measured with the microscope the photoluminescence of the hybrid structure as a function of the emission angle by imaging the back focal plane of the objective. The precise tuning of the dimensions of the metallic elements of the nanoantenna leads to a strong variation of the directionality of the emission, being able to change this emission from backward to forward. We explain the mechanism leading to this directional emission by finite difference time domain simulations of the scattering efficiency of the antenna elements. These results cast the first step toward the realization of electrically driven optical Yagi-Uda antenna emitters based on semiconductor nanowires.

KEYWORDS: Semiconductor nanowire, Yagi-Uda optical antenna, directional emission, Fourier microscopy



Because of the unique optical properties of semiconductor nanowires they are an excellent platform for optoelectronic and photonic applications.^{1–3} The possibility of controlling their composition, geometry, and crystallographic morphology opens up a great freedom in designing different devices with desired properties.⁴ In recent years, several studies have been realized on optically⁵ and electrically⁶ driven nanolasers, solar cells,^{7–9} optical switches,¹⁰ and single photon sources coupled to optical waveguides.^{11,12} The photoluminescence properties of nanowires and the coupling of their emission to leaky and guided modes have been studied extensively.^{13–17} In addition, the coupling of nanowires with plasmonic nanostructures modifies their optical properties.^{18–20} In parallel, in the past decade many efforts have been done to enhance the efficiency and modify the direction of the emission of quantum emitters including quantum dots and fluorescent molecules.^{21–25} Yagi-Uda optical antennas are an example of a structure showing a pronounced directionality of the emission.^{24,26–31} In this system, the emission of a single quantum emitter couples to the antenna feed element, which is a metallic nanorod acting as a half-wavelength dipole nanoantenna. The permittivity of noble metals, including Au, Ag, and Al, and the size of the nanorods leads to plasmonic resonances in the visible range of the electromagnetic spectrum. These resonances modify the spontaneous emission rate of nearby emitters due to the change of the local density of optical states.³² Subsequently, the scattering of the feed element emission with the antenna elements and the interference of this

scattered radiation in the far-field leads to a strong directional emission. This emission can be controlled by the resonant response of the elements forming the Yagi-Uda antenna and their spacing.

In this Letter, we demonstrate a hybrid semiconductor–metal Yagi-Uda antenna. This hybrid system is realized by replacing the resonant metallic feed element of the Yagi-Uda by a nonresonant semiconductor nanowire. As we show, the nonresonant emission from the nanowire is not a limitation for the strong directional emission of the Yagi-Uda antenna. The measurements have been performed on GaAs nanowires using a Fourier microscope, that is, a microscope that images the reciprocal space or the angular distribution of the emission. To demonstrate the strong dependence of the emission with the antenna parameters, we have fabricated two devices with different dimensions to direct the emission in opposite directions. The mechanism leading to the directional emission is studied by means of the finite difference time domain (FDTD) method and explained in terms of the scattering efficiencies of the antenna elements. The results of this Letter can be exploited for the development of electronically driven optical Yagi-Uda antennas for directional single photon emission. The schematic representation of the nanowire–Yagi-Uda hybrid system is shown in Figure 1a. The antenna is

Received: February 10, 2015

Revised: June 1, 2015

Published: June 18, 2015

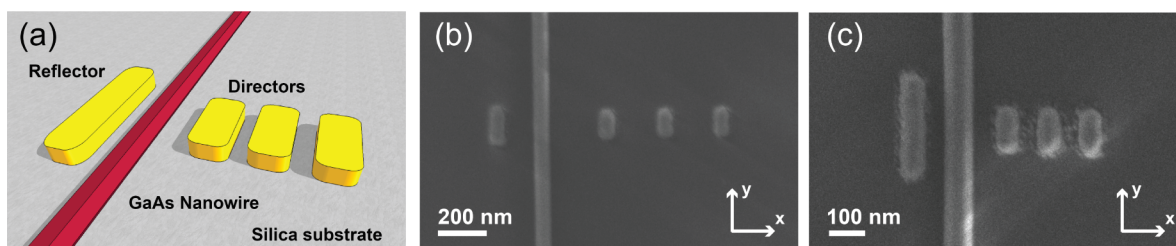


Figure 1. (a) Schematic representation of an hybrid nanowire–plasmonic Yagi-Uda antenna. The nanowire is represented by the long red structure, while the plasmonic reflector and directors are represented by the yellow rods. All structures are fabricated on silica substrates. (b,c) SEM images of the hybrid nanowire-Yagi-Uda optical antennas. (b) Corresponds to YU175 with the reflector length of 175 nm and (c) to YU300 with the reflector length of 300 nm.

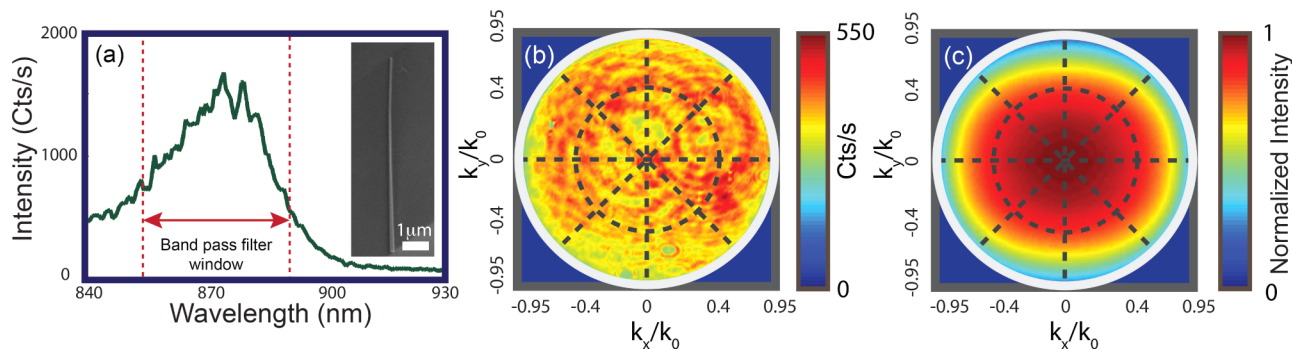


Figure 2. (a) Photoluminescence spectrum of a GaAs nanowire with diameter of 70 ± 5 nm. The SEM image of the nanowire on the silica substrate is shown in the inset of panel (a). The dotted lines indicate the bandwidth of a filter used to collect only the nanowire emission in the Fourier measurements. (b) Radiation pattern of a GaAs nanowire in Fourier space. A relatively homogeneous emission across the Fourier plane can be seen. The light gray circle represents the collection angle of the objective with a numerical aperture of 0.95. (c) Simulation of the radiation pattern of a GaAs nanowire on a silica substrate. The simulated emission is normalized by its maximum value.

formed by a GaAs nanowire (red bar in Figure 1a) acting as feed element of the emission; three metal rods acting as directors, and a bigger metal rod on the opposite side of the nanowire acting as reflector. The role of the directors is to beam the emission of reflector–nanowire pair into smaller solid angles toward their side. This solid angle is determined by the number of directors. Hybrid Yagi-Uda antennas were fabricated by the procedure explained in detail in Methods. Scanning electron microscopy (SEM) images of the two investigated antennas are shown in Figure 1b,c. The main difference between the antennas are the length of the reflectors and the distance between the elements. Detailed information on the dimensions of the antennas is available in Methods. We name these antennas as YU175 (Figure 1b) and YU300 (Figure 1c) in reference to the length of their directors, which are 175 and 300 nm, respectively. Note that the distance between the semiconductor nanowire and the metallic rods is relatively large (>100 nm). Therefore, we do not expect to have any strong modification of the luminescence decay rate in this system.^{21,22,28}

We have used Fourier microscopy to measure the directionality of the emission from the hybrid Yagi-Uda.³³ The schematic representation of the setup is shown in Figure S1 (Supporting Information). The nanowire is excited with a focused beam (fwhm ≈ 650 nm) from a continuous wave laser diode ($\lambda = 785$ nm) by means of a $100\times$ objective with a numerical aperture of 0.95. The illuminated power for all experiments is kept constant and equal to 25 mW. The photoluminescence is collected by the same objective and decomposed on the back focal plane of the objective in its plane wave components, each with a defined wave vector. This plane

is imaged by the Fourier lens located at the distance $2f$, where f is its focal length. A charge-coupled device (CCD) camera is positioned at the distance $2f$ from the Fourier lens to obtain the image of the back focal plane of the objective. To detect only the emission of GaAs nanowires and to filter out the scattered light from the excitation laser, a band-pass filter, 880 ± 20 nm, followed by a notch filter at 785 nm were placed in front of the CCD camera.

The photoluminescence spectrum of a bare GaAs nanowire at room temperature is shown in Figure 2a. The peaked emission at $\lambda \sim 870$ nm is characteristic of GaAs nanowires. The SEM image of this nanowire is displayed in the inset of Figure 2a. The Fourier emission pattern obtained from the bare nanowire is shown in Figure 2b. The Fourier image represents the measurement of intensity in Cts/s in color scale as a function of the components of the emission wave vector in the plane of the sample (k_x, k_y) normalized by $k_0 = 2\pi/\lambda$. The light gray circle in the figure indicates the acceptance angle of the objective with a numerical aperture of 0.95. This emission exhibits centrosymmetric radiation pattern. The FDTD simulation of the radiation pattern shown in Figure 2c, and described in Methods, is in good agreement with the measurement.

To understand the physics leading to the radiation pattern shown in Figure 2, we have calculated the dispersion of the guided and leaky modes supported by an infinitely long cylinder embedded in homogeneous medium³⁴ (see the Figure S2 in the Supporting Information). The fundamental mode (HE_{11}) is the only guided mode that is supported by GaAs nanowires with a diameter of 70 nm. However, the coupling efficiency of the nanowire emission to this mode is low due to

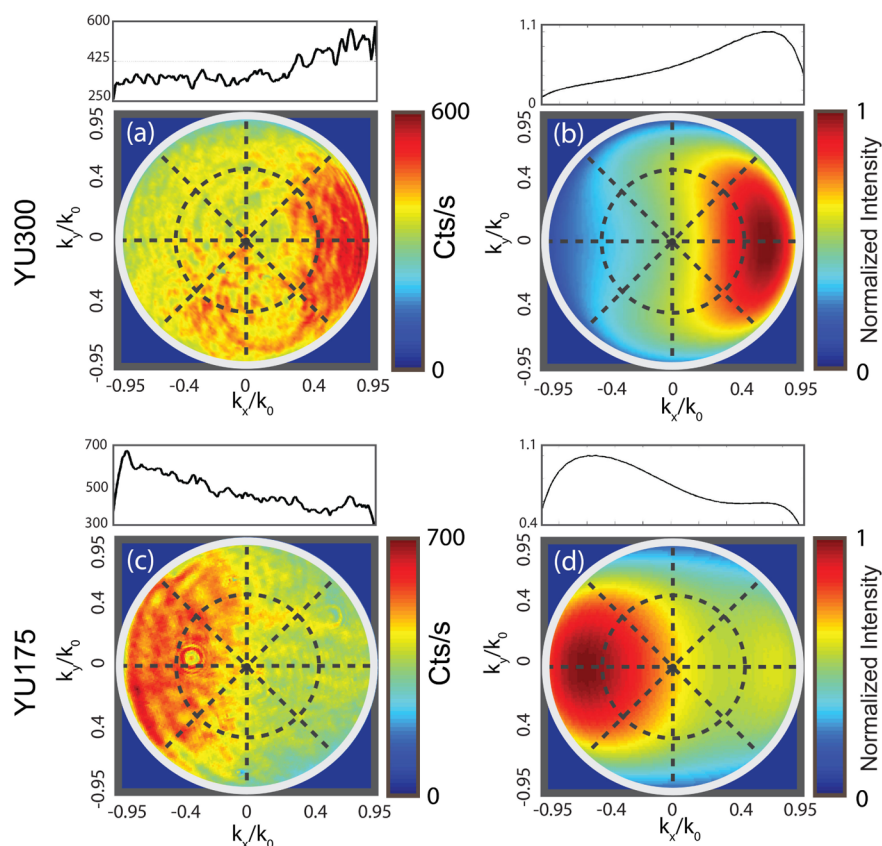


Figure 3. (a) Radiation pattern measurement of YU300. Most of the radiation is directed toward the reflector (right direction). (b) Simulation of the normalized radiation pattern of YU300. (c) Measurement of the radiation pattern from YU175. Most of the emission is directed toward the reflector (left direction). (d) Simulated radiation pattern of YU175 normalized by its maximum.

the mode profile extending mainly in the surrounding medium.¹⁷ Therefore, most of the emission leaks out of the nanowire close to the region where the nanowire is excited.¹⁶ Hence, the far-field radiation pattern of the horizontal nanowire becomes highly nondirectional as shown in Figure 2b. This important characteristic facilitates the coupling of the emission from the nanowire to the metallic elements of the Yagi-Uda antenna.

Figure 3a shows the measurement of the radiation pattern of YU300. A large fraction of the radiation is directed toward the forward direction (the $k_x > 0$ direction), that is, the directionality of the emission is toward the side of the directors of the Yagi-Uda antenna. Furthermore, a strong beaming that confines the emission in the range of $-0.4 < k_y/k_0 < 0.4$ can be seen. The FDTD simulation of the radiation pattern of this antenna is shown in Figure 3b and confirms the measurements with an excellent agreement. The effect of the reflector length on the directionality of the antenna emission is experimentally shown in Figure 3c. By decreasing the length of the reflector element to 175 nm in YU175, the emission points toward the backward direction, that is, the $k_x < 0$ direction. Moreover, a weaker directionality and beaming of the emission are obtained in this device.

One criterion in the assessment of the antenna performance is the front-to-back emission ratio (F/B). This factor is defined as the ratio between the emission intensity along the radiation direction defined by the directors ($k_x > 0$ in our antenna) and the intensity at the opposite direction. The F/B ratio for YU300 determined at $k_x/k_0 = 0.83$, that is, the wave vector of maximum emission, is 1.8 for the experiment and 4 in the

simulation. The difference between the experimental and theoretical F/B values can be attributed to the background intensity in the far-field radiation pattern originating from the excitation of the nanowire. As discussed in Methods, to simulate the radiation pattern of the devices a single electrical dipole is placed in the middle of the nanowire, oriented along its long axis.^{35,36} Consequently, a very localized excitation of the emission is considered for the simulations. However, in experiments the nanowire is excited by a diffraction-limited focused laser spot. This illumination excites regions of the nanowire relatively far from the Yagi-Uda elements and introduces a background intensity in the directional emission pattern. Another source that can lead to the background emission is the excitons diffusion along the nanowire. Typical exciton diffusion length for these type of GaAs nanowires is $< 1 \mu\text{m}$.³⁷ This is comparable with the size of the excitation beam. Therefore, it is not possible to distinguish from the measurements what the origin of the emission background is. However, this background could be significantly reduced if embedded heterostructures or quantum dots are used as the emission source. For YU175, the F/B ratios defined at the same k_x/k_0 as for YU300 are 0.48 (experiment) and 0.62 (simulation). These F/B ratios smaller than 1 indicate beaming of the emission along the wrong direction. The response of YU175 is thus dominated by the large scattering efficiency of the reflector, resulting for its resonant behavior at the nanowire emission wavelength, and the directors do not have a significant influence on the emission directionality.

In order to give a simple description in the mechanism leading to the pronouncedly different directionality of the

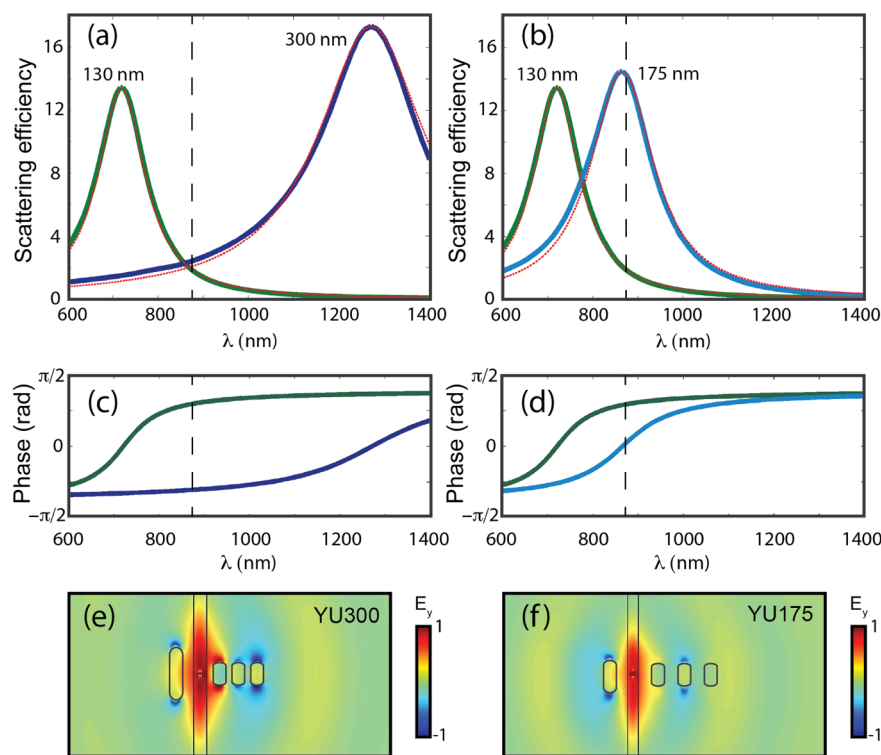


Figure 4. Numerical simulations of the scattering efficiency of Au rods with a height of 50 nm and a width of 60 nm on a silica substrate. (a) Simulation of two rods with lengths of 130 and 300 nm representing the directors and reflector of YU300. (b) As in (a) but for rods with a length of 130 and 175 nm representing the directors and reflector of YU175, respectively. The emission peak of the GaAs nanowire ($\lambda = 870$ nm) is indicated by the black dashed line in both panels. The red dotted curves are Lorentzian fits to the scattering efficiency simulations. (c,d) The calculated phase of the Lorentzian oscillators in panels (a) and (b), respectively. (e,f) Snapshots from the FDTD simulation of the normalized amplitude of the y -component of the electric near-field in YU175 and YU300, respectively.

emission of different antennas, we have numerically calculated the scattering efficiency of Au rods with the dimensions of the antenna elements, that is, width of 60 nm, height of 50 nm, and with different lengths, placed on a silica substrate. The length of the rod is varied between 130 to 300 nm. The scattering efficiency is defined as the scattering cross section normalized by the geometrical cross section of the rod. The metallic rod is illuminated at normal incidence by a polarized plane wave along the length of the rod. The calculated values of the scattering efficiency are shown in Figure 4a,b for the director and reflector rods of YU300 and YU175, respectively. The corresponding absorption efficiencies are given in Figure S3 in the Supporting Information. These absorption efficiencies are ≈ 5 times lower than the scattering efficiencies. Therefore, the dominant mechanism leading to the directional emission can be ascribed to scattering. The scattering efficiency exhibits the characteristic resonant behavior due to a localized surface plasmon polariton, that is, the coherent oscillation of the free electrons in the metallic rod. These resonances correspond to the lowest order plasmonic mode, that is, the $\lambda/2$ resonance. As expected, a considerable redshift of the resonance frequency occurs by increasing the length of the rod. The scattering efficiency of each rod can be considered as a reliable criteria for selecting the proper geometrical parameters to control the directional emission of a Yagi-Uda antenna.²⁶ In Figure 4a, that is, YU300, the length of the directors and the reflector are 130 and 300 nm, respectively. At the emission wavelength of the nanowire, $\lambda = 870$ nm (vertical dashed line), both rods are off-resonance. The resonance frequency for the 130 nm rod is at a shorter wavelength, while it is at a longer wavelength for the

300 nm rod. However, the scattering efficiency is similar for both rods at 870 nm. In YU175, (Figure 4 b), the longer rod, that is, the reflector, is at resonance at $\lambda = 870$ nm by setting its length to 175 nm. Consequently, the scattering efficiency for this element is ~ 7 times larger than for the shorter rods, that is, the directors.

The scattering efficiency simulations have been fitted to Lorentzian functions (red dotted curves in Figure 4a,b) describing the harmonic charge oscillation of the surface plasmons in order to estimate the phase difference between the induced polarization vector and the incident electric field. In Figure 4c,d, the Lorentz oscillator phase is represented for the rods of YU300 and YU175, respectively. In YU300, (Figure 4c) at $\lambda = 870$ nm the charge oscillation in the rods with the length of 130 nm (director) and 300 nm (reflector) are approximately in antiphase with respect to each other; while, for YU175 (Figure 4d) the relative phase difference between director and reflectors is much smaller.

In YU175, the amplitude of the scattered field by the rods leads to strong scattering by the reflector and relatively weak scattering by the directors. This difference in scattering efficiency, together with the relative phase of the scattered field by the reflector and the directors, prevents the scattered field from the reflector element to destructively interfere with the emission of the nanowire along the backward direction. However, when the length of the reflector element is 300 nm, the resonance frequency is significantly redshifted with respect to the emission peak of nanowire at $\lambda = 870$ nm. Hence, the scattering efficiencies of the reflector and directors are similar at the nanowire emission wavelength. This condition, together

with the antiphase oscillation of the localized surface plasmons, leads to the effective cancellation of the emission from the nanowire in the backward direction.

The spectral difference between the resonance peaks in Figure 4a,b for the reflectors and directors shows a flexible range of operational wavelengths for the emitting element. Because the emission peak of the GaAs nanowire is centered at $\lambda = 870$ nm, we do not have the possibility of varying this wavelength. However, changing GaAs to other materials will still lead to significant directionality as long as the emission is in the range where the scattering efficiencies of reflector and directors are similar.

The full three-dimensional (3D) simulation of the antenna emission and the electric field components originating from an electric dipole embedded in the nanowire can provide deeper insight regarding the performance of the antennas. Figure 4e,f shows snap-shots of the near field amplitude in the xy plane of the E_y electric field component. This is the dominant field component of the emission for YU300 and YU175, respectively. The first conspicuous feature related to the performance of the antennas is the phase difference between reflector and the directors that can be appreciated qualitatively by the color coded E_y . The temporal evolution of the electric field shows that in one period of oscillation of the radiating dipole in YU175 the phase difference between the reflector and first director is similar as described earlier. This does not provide the proper interference condition for beaming in the forward direction. On the contrary, for YU300 the phase difference between these two elements provides a destructive interference on the backward direction and beaming in the forward direction. An animation of scattered near-fields for the two different designs is provided in the Supporting Information.

In conclusion, we have demonstrated strong directional emission of GaAs nanowires by coupling this emission to a Yagi-Uda nanoantenna fabricated around the nanowire. This structure forms a hybrid metallic–semiconductor optical antenna. We have also demonstrated that the directionality of the emission can be modified by varying the size of the elements forming the antenna. FDTD simulations of the emission shows excellent agreement with the experimental data. The mechanism leading to this directionality is explained by calculation of scattering efficiencies of the individual metallic elements of the antenna and by full electrodynamic 3D simulations of the full structures. These results constitute the first steps toward the realization of electrically driven directional antennas based on semiconductor nanowires.

Methods. Fabrication. We have used thin (diameter <100 nm) nanowires to minimize the coupling of the emission to guided modes supported by the nanowire.¹⁷ Because of the recent advancement of the semiconductor growth technology, GaAs nanowires with a high degree of control on the geometry and the doping concentration can be achieved.³⁸ The GaAs nanowires were grown on Si(111) undoped wafer via Ga-assisted method in DCA P600 solid source MBE machine. A Ga rate of 0.3 Å/s as flux of 2.5×10^{-6} Torr and a substrate temperature of 640 °C was used for the growth process. During growth, the substrate was rotated by 7 rpm and a V/III beam equivalent pressure ratio of 50. Applying these conditions give rise to the growth of nanowires with a diameter of 55 nm and length of approximately 12 μm . After the growth of the nanowire core, a 4 nm layer of $\text{Al}_x\text{Ga}_{1-x}\text{As}$ ($x = 0.3$) and another 3 nm capping layer of GaAs were grown by changing

the growth conditions to the “two-dimensional epitaxy”.³⁹ The presence of $\text{Al}_x\text{Ga}_{1-x}\text{As}$ layer passivates the core of the nanowire and decreases the destructive nonradiative surface recombination.^{40–43} At the end of the process, the final diameter of the nanowire is ~ 70 nm. The nanowires were removed from the as-grown silicon substrate in an isopropanol solution by ultrasonic bath for 1 min. A few drops of the isopropanol solution containing nanowires were transferred to a patterned fused silica substrate. After the dispersion of the nanowires on the substrate, the position of the nanowires was recognized with optical microscopy. Each area on the patterned substrate encoded the relative position of the nanowire on the wafer. The nanoantennas around the individual nanowires were designed by custom-made software and translated to the files to write e-beam structures. The final position of the nanowires was assigned by a “shape recognition algorithm” giving rise to position accuracy of less than 50 nm.⁴⁴ The substrate was spin coated by a double resist layer of methyl methacrylate and poly(methyl methacrylate) and 10 nm of Cr was evaporated on top of the resist in order to discharge the charge accumulation during e-beam lithography. After the lithography step, Cr was etched and the evaporation of 5 nm Ti and 50 nm Au was performed. The presence of Ti improves the adhesion of gold to the silica substrate.

Table 1 shows the geometrical dimensions of the antenna elements measured by SEM. It should be noted that all the

Table 1. Dimensions of the Fabricated Yagi-Uda + Nanowire Hybrid Antennas^a

antenna	d_{nw}	L_r	L_d	w	a_r	a_d	L_{total}
YU175	75	175	130	60	185	205	860
YU300	75	300	130	60	155	120	575

^aAll the dimensions are in nanometers.

measurements on bare nanowire, YU175 and YU300 are done on separate nanowires taken from the same growth batch. d_{nw} is the diameter of nanowire, L_r and L_d are the lengths of the reflector and directors, respectively, w is the width of the metallic rods, a_r is the distance between the center of the reflector to the center of the nanowire, and a_d is the distance between the center of the director to the center of the nanowire and the distance between the directors.

Numerical Simulations. The simulations of the radiation patterns were performed with the FDTD method (Lumerical’s FDTD Solution). The GaAs nanowire with the length of 6 μm and the diameter of 70 nm is placed horizontally on top of a silica substrate. The medium on top of the substrate is considered to be air ($n = 1$). The optical constants of GaAs were taken from Palik.⁴⁵ An oscillating electrical dipole along the long axis of the nanowire is considered as the emission source. The near-field components of the electric field were detected by a planar monitor parallel to the substrate. The far-field patterns were calculated using the near-field to far-field conversion method.

■ ASSOCIATED CONTENT

Supporting Information

Supporting Information shows the schematic representation of the Fourier setup, dispersion of the leaky and guided modes in GaAs nanowires, absorption and scattering efficiencies of the antenna elements, effect of the number of directors on the directionality, near-field map of intensity enhancement, and

animations of the y -component of scattered near-fields for two different antennas. The Supporting Information is available free of charge on the ACS Publications website at DOI: 10.1021/acs.nanolett.5b00565.

AUTHOR INFORMATION

Corresponding Authors

*E-mail: anna.fontcuberta-morrall@epfl.ch.

*E-mail: rivass@amolf.nl.

Notes

The authors declare no competing financial interest.

ACKNOWLEDGMENTS

We thank Sander Mann for the careful checking of the manuscript. This work has been implemented under the support of Schweizerischer Nationalfonds (SNF) through project numbers 137648 and 156081, European Union's Initial Training Networks (ITN), Netherlands Foundation for Fundamental Research on Matter (FOM), and The Netherlands Organization for Scientific Research (NWO) and is part of an industrial partnership program between Philips and FOM.

REFERENCES

- (1) Li, Y.; Qian, F.; Xiang, J.; Lieber, C. M. Nanowire electronic and optoelectronic devices. *Mater. Today* **2006**, *9*, 18–27.
- (2) Yan, R.; Gargas, D.; Yang, P. Nanowire photonics. *Nat. Photonics* **2009**, *3*, 569–576.
- (3) Yang, P.; Yan, R.; Fardy, M. Semiconductor Nanowire: What's Next? *Nano Lett.* **2010**, *10*, 1529–1536.
- (4) Thelander, C.; Agarwal, P.; Brongersma, S.; Eymery, J.; Feiner, L.; Forchel, A.; Scheffler, M.; Riess, W.; Ohlsson, B.; Gösele, U.; Samuelson, L. Nanowire-based one-dimensional electronics. *Mater. Today* **2006**, *9*, 28–35.
- (5) Saxena, D.; Mokkalapati, S.; Parkinson, P.; Jiang, N.; Gao, Q.; Tan, H. H.; Jagadish, C. Optically pumped room-temperature GaAs nanowire lasers. *Nat. Photonics* **2013**, *7*, 963–968.
- (6) Duan, X.; Huang, Y.; Agarwal, R.; Lieber, C. M. Single-nanowire electrically driven lasers. *Nature* **2003**, *421*, 241–245.
- (7) Kelzenberg, M. D.; Boettcher, S. W.; Petykiewicz, J. A.; Turner-Evans, D. B.; Putnam, M. C.; Warren, E. L.; Spurgeon, J. M.; Briggs, R. M.; Lewis, N. S.; Atwater, H. A. Enhanced absorption and carrier collection in Si wire arrays for photovoltaic applications. *Nat. Mater.* **2010**, *9*, 239–244.
- (8) Krogstrup, P.; Jorgensen, H. I.; Heiss, M.; Demichel, O.; Holm, J. V.; Aagesen, M.; Nygard, J.; Fontcuberta i Morral, A. Single-nanowire solar cells beyond the Shockley-Queisser limit. *Nat. Photonics* **2013**, *7*, 306–310.
- (9) Wallentin, J.; Anttu, N.; Asoli, D.; Huffman, M.; Åberg, I.; Magnusson, M. H.; Siefert, G.; Fuss-Kailuweit, P.; Dimroth, F.; Witzigmann, B.; Xu, H. Q.; Samuelson, L.; Deppert, K.; Borgström, M. T. InP Nanowire Array Solar Cells Achieving 13.8 Ray Optics Limit. *Science* **2013**, *339*, 1057–1060.
- (10) Piccione, B.; Cho, C.-H.; van Vugt, L. K.; Agarwal, R. All-optical active switching in individual semiconductor nanowires. *Nat. Nanotechnol.* **2012**, *7*, 640–645.
- (11) Claudon, J.; Bleuse, J.; Malik, N. S.; Bazin, M.; Jaffrennou, P.; Gregersen, N.; Sauvan, C.; Lalanne, P.; Gerard, J.-M. A highly efficient single-photon source based on a quantum dot in a photonic nanowire. *Nat. Photonics* **2010**, *4*, 174–177.
- (12) Bulgarini, G.; Reimer, M. E.; Bouwes Bavinck, M.; Jöns, K. D.; Dalacu, D.; Poole, P. J.; Bakkers, E. P. A.; Zwiller, V. Nanowire Waveguides Launching Single Photons in a Gaussian Mode for Ideal Fiber Coupling. *Nano Lett.* **2014**, *14*, 4102–4106.
- (13) Maslov, A. V.; Ning, C. Z. Far-field emission of a semiconductor nanowire laser. *Opt. Lett.* **2004**, *29*, 572–574.

(14) Maslov, A. V.; Bakunov, M. I.; Ning, C. Z. Distribution of optical emission between guided modes and free space in a semiconductor nanowire. *J. Appl. Phys.* **2006**, *99*, -.

(15) Cao, L.; White, J. S.; Park, J.-S.; Schuller, J. A.; Clemens, B. M.; Brongersma, M. L. Engineering light absorption in semiconductor nanowire devices. *Nat. Mater.* **2009**, *8*, 643–647.

(16) Grzela, G.; Paniagua-Domínguez, R.; Barten, T.; Fontana, Y.; Sánchez-Gil, J. A.; Gómez Rivas, J. Nanowire Antenna Emission. *Nano Lett.* **2012**, *12*, 5481–5486.

(17) Paniagua-Dominguez, R.; Grzela, G.; Rivas, J. G.; Sanchez-Gil, J. A. Enhanced and directional emission of semiconductor nanowires tailored through leaky/guided modes. *Nanoscale* **2013**, *5*, 10582–10590.

(18) Muskens, O. L.; Treffers, J.; Forcales, M.; Borgström, M. T.; Bakkers, E. P. A. M.; Rivas, J. G. Modification of the photoluminescence anisotropy of semiconductor nanowires by coupling to surface plasmon polaritons. *Opt. Lett.* **2007**, *32*, 2097–2099.

(19) Brittman, S.; Gao, H.; Garnett, E. C.; Yang, P. Absorption of Light in a Single-Nanowire Silicon Solar Cell Decorated with an Octahedral Silver Nanocrystal. *Nano Lett.* **2011**, *11*, 5189–5195.

(20) Casadei, A.; Pecora, E. F.; Trevino, J.; Forestiere, C.; Rüffer, D.; Russo-Averchi, E.; Matteini, F.; Tutuncuoglu, G.; Heiss, M.; Fontcuberta i Morral, A.; Dal Negro, L. Photonic-Plasmonic Coupling of GaAs Single Nanowires to Optical Nanoantennas. *Nano Lett.* **2014**, *14*, 2271–2278.

(21) Anger, P.; Bharadwaj, P.; Novotny, L. Enhancement and Quenching of Single-Molecule Fluorescence. *Phys. Rev. Lett.* **2006**, *96*, 113002.

(22) Kühn, S.; Håkanson, U.; Rogobete, L.; Sandoghdar, V. Enhancement of Single-Molecule Fluorescence Using a Gold Nanoparticle as an Optical Nanoantenna. *Phys. Rev. Lett.* **2006**, *97*, 017402.

(23) Muskens, O. L.; Giannini, V.; Sánchez-Gil, J. A.; Gómez Rivas, J. Strong Enhancement of the Radiative Decay Rate of Emitters by Single Plasmonic Nanoantennas. *Nano Lett.* **2007**, *7*, 2871–2875.

(24) Curto, A. G.; Volpe, G.; Taminiau, T. H.; Kreuzer, M. P.; Quidant, R.; van Hulst, N. F. Unidirectional Emission of a Quantum Dot Coupled to a Nanoantenna. *Science* **2010**, *329*, 930–933.

(25) Novotny, L.; van Hulst, N. Antennas for light. *Nat. Photonics* **2011**, *5*, 83–90.

(26) Li, J.; Salandrino, A.; Engheta, N. Shaping light beams in the nanometer scale: A Yagi-Uda nanoantenna in the optical domain. *Phys. Rev. B* **2007**, *76*, 245403.

(27) Hofmann, H. F.; Kosako, T.; Kadoya, Y. Design parameters for a nano-optical Yagi-Uda antenna. *New J. Phys.* **2007**, *9*, 217.

(28) Koenderink, A. F. Plasmon Nanoparticle Array Waveguides for Single Photon and Single Plasmon Sources. *Nano Lett.* **2009**, *9*, 4228–4233.

(29) Kosako, T.; Kadoya, Y.; Hofmann, H. F. Directional control of light by a nano-optical Yagi-Uda antenna. *Nat. Photonics* **2010**, *4*, 312–315.

(30) Coenen, T.; Vesseur, E. J. R.; Polman, A.; Koenderink, A. F. Directional Emission from Plasmonic Yagi-Uda Antennas Probed by Angle-Resolved Cathodoluminescence Spectroscopy. *Nano Lett.* **2011**, *11*, 3779–3784.

(31) Dorfmueller, J.; Dregely, D.; Esslinger, M.; Khunsin, W.; Vogelgesang, R.; Kern, K.; Giessen, H. Near-Field Dynamics of Optical Yagi-Uda Nanoantennas. *Nano Lett.* **2011**, *11*, 2819–2824.

(32) Novotny, L.; Hecht, B. *Principles of Nano-Optics*, 2nd ed.; Cambridge University Press: New York, 2012.

(33) Fontana, Y.; Grzela, G.; Bakkers, E.; Rivas, J. Mapping the directional emission of quasi-two-dimensional photonic crystals of semiconductor nanowires using Fourier microscopy. *Phys. Rev. B* **2012**, *86*, 245303.

(34) Stratton, J. A. *Electromagnetic Theory. International Series in Pure and Applied Physics*; McGraw-Hill Book Company: New York, 1941.

(35) Wang, J.; Gudiksen, M. S.; Duan, X.; Cui, Y.; Lieber, C. M. Highly Polarized Photoluminescence and Photodetection from Single Indium Phosphide Nanowires. *Science* **2001**, *293*, 1455–1457.

(36) Rümke, T. M.; Sánchez-Gil, J. A.; Muskens, O. L.; Borgström, M. T.; Bakkers, E. P.; Rivas, J. G. Local and anisotropic excitation of surface plasmon polaritons by semiconductor nanowires. *Opt. Express* **2008**, *16*, 5013–5021.

(37) Bolinsson, J.; Mergenthaler, K.; Samuelson, L.; Gustafsson, A. Diffusion length measurements in axial and radial heterostructured nanowires using cathodoluminescence. *J. Cryst. Growth* **2011**, *315*, 138–142.

(38) Dufouleur, J.; Colombo, C.; Garma, T.; Ketterer, B.; Uccelli, E.; Nicotra, M.; Fontcuberta i Morral, A. P-Doping Mechanisms in Catalyst-Free Gallium Arsenide Nanowires. *Nano Lett.* **2010**, *10*, 1734–1740.

(39) Heigoldt, M.; Arbiol, J.; Spirkoska, D.; Rebled, J. M.; Conesa-Boj, S.; Abstreiter, G.; Peiro, F.; Morante, J. R.; Fontcuberta i Morral, A. Long range epitaxial growth of prismatic heterostructures on the facets of catalyst-free GaAs nanowires. *J. Mater. Chem.* **2009**, *19*, 840–848.

(40) Titova, L. V.; Hoang, T. B.; Jackson, H. E.; Smith, L. M.; Yarrison-Rice, J. M.; Kim, Y.; Joyce, H. J.; Tan, H. H.; Jagadish, C. Temperature dependence of photoluminescence from single core-shell GaAs-AlGaAs nanowires. *Appl. Phys. Lett.* **2006**, *89*, 253101.

(41) Demichel, O.; Heiss, M.; Bleuse, J.; Mariette, H.; Fontcuberta i Morral, A. Impact of surfaces on the optical properties of GaAs nanowires. *Appl. Phys. Lett.* **2010**, *97*, 251101.

(42) Casadei, A.; Schwender, J.; Russo-Averchi, E.; Rüffer, D.; Heiss, M.; Alarcó-Lladó, E.; Jabeen, F.; Ramezani, M.; Nielsch, K.; Morral, A. F. i. Electrical transport in C-doped GaAs nanowires: surface effects. *Phys. Status Solidi RRL* **2013**, *7*, 890–893.

(43) Joyce, H. J.; Docherty, C. J.; Gao, Q.; Tan, H. H.; Jagadish, C.; Lloyd-Hughes, J.; Herz, L. M.; Johnston, M. B. Electronic properties of GaAs, InAs and InP nanowires studied by terahertz spectroscopy. *Nanotechnology* **2013**, *24*, 214006.

(44) *qstarter by NCCR QSIT*; <http://www.qstarter.ch/projects/automated-contacting-of-random-microstructures>, accessed Jan 2014.

(45) Palik, E. D. *Handbook of Optical Constants of Solids*; Academic Press: New York, 1998.